RSC Advances

ROYAL SOCIETY OF CHEMISTRY

www.rsc.org/advances

Synthesizing MgO with high specific surface for carbon dioxide adsorption

Yu-Dong Ding, Gan Song, Xun Zhu*, Rong Chen, Qiang Liao

[1]*Key Laboratory of Low-grade Energy Utilization Technologies and Systems (Chongqing University), Ministry of Education, Chongqing, 400030, China*

[2]*Institute of Engineering Thermophysics, Chongqing University, Chongqing 400030, China*

Abstract

In this work, highly porous MgO was synthesized for CO_2 adsorption by a simple and economic thermal decomposition of basic magnesium carbonate and magnesium oxalate. Characterizations of the synthesized samples were accomplished using scanning electron microscopy (SEM), powder X-ray diffraction (XRD), and nitrogen adsorption-desorption isotherm. The results showed that the synthesized MgO possessed a high BET surface area in a range of 161-252 m^2g^{-1} and a highly porous structure. Thermo gravimetric analysis revealed that the synthesized MgO not only showed good selectivity to CO_2 but also yielded a CO_2 adsorption capacity of as high as 7.59 wt%. Besides, in situ FTIR spectroscopy and CO_2 TPD curves demonstrated that the adsorption mechanism of synthesized MgO was mainly attributable to chemisorption and it could be regenerated at relatively low temperature. This work provides a new way to synthesize MgO with highly porous structure for CO_2 adsorption.

Keywords: Porous MgO, CO_2 adsorption, thermal decomposition, high surface area

1. Introduction

Nowadays, climate change is gaining more and more attention all over the world. According to report by the intergovernmental panel on climate change (IPCC), the global temperature will rise 1.9 °C by 2100[1, 2]. CO_2 is the main source of anthropogenic greenhouse gas which makes a significant contribution to the global warming. It is estimated that CO_2 contributes 55% to the global temperature rise[3]. Among CO_2 emission sources, fossil fuel power plants are the largest anthropogenic source, accounting for nearly one-third of the total CO_2 emission.[4] Consequently, it is urgent to migrate the CO_2 emission from fossil fuel power plants. Adsorption method

is one of the most promising CO_2 capture technologies as it possesses a number of advantages, such as no liquid waste, low regeneration energy requirement, wide range of operating temperature and so on[5]. To date, a series of materials have been researched for the adsorption of CO_2 such as carbon-based materials[6], zeolites[7], hydrotalcite-like compounds[8], metal oxides[9] and metal organic frameworks[10]. Among these materials, MgO has been receiving ever-increasing attention because it can offer many striking features. First of all, MgO can adsorb CO_2below 200 °C and be regenerated at relatively low temperature compared with conventionally-used CaO[11, 12]. Secondly, MgO is suitable to adsorb CO_2 in the presence of H_2O without reducing the CO_2 adsorption capacity[13]. Furthermore, Mg-based minerals are widely available in nature and can be prepared in large amount with low cost. Hence, all these features make MgO particularly suitable for the capture of CO_2 emitted from fossil fuel power plants.

Although promising, the CO_2 adsorption capacity of pure MgO is still fairly small (~2 wt%)[14] due to the low specific surface. Previous studies also indicate that the CO_2 adsorption capacity of MgO is inherently correlated with its specific surface area,[15, 16]and an increase in the specific surface area can improve the adsorption performance. As a result, the synthesis of porous MgO with high specific surface area has been recognized to be an effective way to increase the CO_2 adsorption capacity of MgO by decreasing the particle size and increasing the active sites such as edges and corners on the crystalline structure[17]. In the past, extensive efforts have been devoted to the preparation of the MgO with a good porous structure. The most conventional way to synthesize porous MgO is the sol-gel method[18]. In addition, several other preparation methods have also been proposed. For instance, Ouraipryvan et al. synthesized highly crystalline MgO nanoparticles with mesoporous-assembled structure via a modified sol-gel process with the aid of surfactant laurylamine hydrochloride as a templating agent[19]. Bhagiyalakshmi et al. synthesized mesoporous magnesium oxide using mesoporous carbon CMK-3 obtained from mesoporous SBA-15 as exotemplate[14]. Zhao et al. synthesized MgO nano/microparticles with multiple morphologies and porous structures via the surfactant assisted solvo- or hydrothermal route in a

dodecylamine or oleic acid solvent[15]. Han et al. synthesized foam-like magnesia materials via one-pot pathway using P123 and PEO as templates and magnesium nitrate as precursor[20]. However, despite the above methods successfully synthesized porous MgO with high specific surface area, these synthesis methods that contain multiple steps of processing the precursor are generally costly and time consuming. At the same time, an expensive or toxic solvent needs to be removed in subsequent preparation steps, which makes the method complex and time consuming. These drawbacks hinder the application of porous MgO in CO_2 adsorption. Consequently, an easy and economical method synthesizing porous MgO with high specific surface area is required to advance the application of MgO in CO_2 adsorption.

In this article, therefore, mesoporous MgO with high specific surface area was synthesized via simple and economical method, in which no expensive or toxic solvent was used. The prepared samples with different structures were characterized by XRD, SEM, surface area and pore size analysis, thermo gravimetric analysis, in situ FTIR and temperature-programed desorption. Besides, a comparison among synthesized MgO and porous MgO reported was made to show the superiority of synthesized MgO in CO_2 adsorption.

2. Experimental methods

Materials

Basic magnesium carbonate (Sigma-Aldrich), magnesium acetate tetrahydrate (Chengdu Kelong Chemical Reagent), ethanedioic acid dehydrate (Chengdu Kelong Chemical Reagent)were used. Commercially available MgO (Chengdu Kelong Chemical Reagent) was also analyzed for comparison.

Preparation of porous MgO

In this work, porous MgO was prepared by the calcination of basic magnesium carbonate. To do this, 5 g of basic magnesium carbonate was calcinated at 400°C for 2 hours with a temperature rising rate of 2 °C/min. This sample was termed as MgO-BMC.

3g of MgO-BMC was then rehydrated by refluxing in distilled water for 3 h. After

centrifugation, the resultant solid was dried at 90 °C for 12 h and then calcinated at 400 °C for 2 hours with a temperature rising rate of 2 °C/min. The achieved sample was termed as MgO-RF.

In addition, porous MgO was also synthesized based on the procedure reported by Bartley et al.[21]0.02 M magnesium acetate tetrahydrate was firstly dissolved in 10 mL distilled water. 0.02 M ethanedioic acid dihydrate was dissolved in 40 mL distilled water. Then, the ethanedioic acid didydrate solution was dropwisely added to the magnesium acetate tetrahydrate solution to form a precipitation and then centrifugated. After centrifugation, the precipitation was dried at 90 °C for 12 h. The obtained solid was calcinated at 400 °C for 2 hours under air environment with a temperature rising rate of 2 °C/min. This sample was termed as MgO-MO. Commercially available MgO used for comparison was termed as MgO-CA.

Characterization of materials

The morphologies of the synthesized samples were obtained using Zeiss AURIGA FIB scanning electron microscopy. Material composition and crystal structure was obtained using XRD pattern by Shimadzu XRD-6000 X-Ray diffractometer with Cu radiation 40 kV and 30 mA. The adsorption-desorption isotherms for nitrogen were determined at -196 °C using an ASAP 2020 surface area and porosity analyzer. BET surface area was then obtained by the Brunauer-Emmett-Teller model. The pore size distribution was obtained from the adsorption branch of the isotherm according to the Barrett-Joyner-Halenda (BJH) method. The total pore volume was determined from the nitrogen amount adsorbed at a relative pressure of 0.97.

CO_2 adsorption

CO_2 adsorption-desorption measurements of the synthesized samples were performed by NETZSCH thermo gravimetric analyzer (STA 409 PC/PG Luxx). In this testing, a sample of 6-8 mg was loaded into an alumina oxide pan and then heated at 400°C for 40 minutes to remove water and impurities adsorbed. Thereafter, the temperature was declined to 50 °C or 100 °C and the adsorption process began. Prior to adsorption, nitrogen (99.8%) was purged with a flowrate of 60 mL/min. After that, carbon dioxide(99.9%) with a flowrate of 100 mL/min was supplied for adsorption. The

adsorption process was carried out under atmospheric pressure for 4 hours and simultaneously the weight changes of the samples were recorded by the analyzer. To investigate the adsorption selectivity to CO_2, a mixture gas with 15% CO_2 and 85% $N_2$was used to replace pure $CO_2$to proceed the same running cycle. For the desorption, the temperature was firstly kept constant at fixed adsorption temperature for 30 minutes, then increased from 50 °C to 450 °C with a temperature rising rate of 3 °C/min to release the CO_2 adsorbed in N_2 environment.

In addition, a Perkin-Elmer Spectrum 100 Series FTIR instrument with a horizontal attenuated total reflectance (HATR) sampling accessory was used for the in situ transmission FTIR spectroscopy to examine the adsorption mechanism of the synthesized samples. Before the measurement, a carbon dioxide feed gas with a flowrate of 20 mL was used to purge the ZnSe crystal for 30 minutes. Then a background spectrum was collected. A sample which was calcinated at 400 °C for 40 minutes to remove impurities was placed on the top of the crystal. The sample was exposed to carbon dioxide for 30 minutes before recording a spectrum. Each spectrum was obtained from 650 cm^{-1} to 4000 cm^{-1} with an instrument resolution of 4 cm^{-1}. To study the surface chemistry of the synthesized samples, an automated chemisorption analyzer (ChemBET Pulsar; Quantachrome Instruments) was used for CO_2 temperature programmed desorption (CO_2-TPD). 0.02 g of MgO sample was loaded into a tubular reactor. The sample was heated at 400 °C for 30 minutes with a purge gas of helium. Then the temperature decreased to 50 °C and CO_2 was charged for 1 hours. During the desorption process, the temperature was raised from 50 °C to 400 °C with a purge gas of 115 mL/min of helium and the desorbed CO_2 was measured continuously.

3. Results and discussion

Characterization of porous MgO

In order to investigate the porous structure of the synthesized samples, XRD, SEM and specific surface area and porosity analyzer were used. Fig. 1 shows the XRD patterns of the synthesized MgO, where the standard XRD patterns of cubic MgO, cubic $Mg(OH)_2$ and cubic $CaCO_3$ are also given for comparison. To clearly observe

the minor peaks of MgO-MO, the XRD pattern of MgO-MO was shown in larger scale compared with the other two samples. The diffraction peaks appeared at 36.9°, 42.9°, 62.3°, 74.7° and 78.6° in standard patterns of MgO. As for MgO-BMC, MgO-MO and MgO-RF, the diffraction peaks at 42.9° and 62.3°, which corresponded to 200 and 220 surface, were found, meaning the cubic MgO in these samples. Moreover, MgO-MO also showed some relatively small diffraction peaks other than the peaks at 42.9° and 62.3°, which demonstrated that MgO-MO sample contained small amount of $Mg(OH)_2$ and trace amount of $CaCO_3$. The tiny $CaCO_3$ may come from the impurity of reagent or the process of sample for XRD test.

The morphologies of the three samples were scanned using SEM as shown in Fig. 2. It can be seen from Fig. 2a that MgO-MO was composed of irregularly cubic-like grain with a distribution of grain size about 500 nm. MgO-BMC (Fig. 2b) was composed of sphere particles with abundant fuzz-like structure on its surface but with the particle size (8 μm) larger than that of MgO-MO. For MgO-RF, after refluxing in water and recalcination, its surface structure was further changed to plate-like structure. This indicated that after refluxing in water, the slice on the surface of MgO particle coalesced and exhibited a smooth surface (Fig. 2c). The morphology of commercially available MgO-CA was also scanned for comparison (Fig. 2d). MgO-CA was composed of irregular particles in the range of 1-2 μm which was larger than that of MgO-MO and no fuzz-like structure on its surface compared with MgO-BMC. From the SEM results, it can be found that the synthesis method had an obvious influence on the morphology of MgO.

To investigate the porous structure of the synthesized samples, N_2 adsorption-desorption isotherms were measured. Fig. 3 shows the N_2 adsorption-desorption isotherms of the three samples. All synthesized samples displayed type IV isotherm with a H3 hysteresis loop according to the IUPAC classification. The hysteresis loop was due to the capillary condensation taking place in mesopores. More importantly, the nitrogen uptake of MgO-MO increased sharply at high relative pressure ($P/P_0>0.6$) compared with the other two synthesized samples, suggesting its highly porous structure. However, MgO-CA exhibited very low

N_2adsorption quantity and non-porous structure. In addition, the pore size distributions of the synthesized samples are also shown in Fig. 3(inset). It can be seen that MgO-MO had a wide range of the pore size distribution, while the pore size distributions were similar and much narrow for MgO-BMC and MgO-RF. Moreover, MgO-MO showed a much higher pore volume per unit pore size compared with MgO-BMC and MgO-RF. This is the reason leading to the high nitrogen uptake at highly relative pressure for MgO-MO. However, all synthesized MgO samples exhibited much higher pore volume compared with commercially available MgO. The detailed information about porous properties of the three samples together with commercially available MgO are listed in Table 1.Clearly, the synthesized MgO samples had much higher BET surface area and pore volume than did commercially available MgO. In particular, the BET surface of MgO-MO could reach as high as 252 m^2g^{-1}, which was almost 8 times of commercially available MgO. But for MgO-BMC, its BET surface area was only about 210 m^2g^{-1}. After rehydrated by refluxing in distilled water, its BET surface area was even decreased to 161 m^2g^{-1}(MgO-RF).These results can be correlated to the variation in morphology by SEM images. Small particle size resulted in a large BET surface area. Besides, after refluxing in water and recalcination, the porous surface of MgO-BMC was changed to smooth surface, thereby lowering the BET surface area. In addition, MgO-MO had the highest pore volume of 0.763cm^3g^{-1} which was nearly 2 times higher than that of MgO-BMC and MgO-RF. The pore size of 12.1 nm was almost double or triple of MgO-BMC and MgO-RF. Therefore, such structure with large surface area and pore volume and size is beneficial not only for CO_2 adsorption but also for the gas transport.

With the above characterization results, it can be known that the MgO was successfully prepared by the thermal decomposition of basic magnesium carbonate and magnesium oxalate. Not only the synthesis procedure was simple and economic but also no toxic or expensive reagent was used, which offers a promising way to synthesize MgO for real applications. More importantly, all of the synthesized samples exhibited good structure with large specific surface area and pore volume compared with commercially available MgO. These features make them to be suited

for CO_2 adsorption.

CO_2 adsorption

To investigate the CO_2 adsorption performance of synthesized MgO, the thermo gravimetric analysis was used. In this work, because CO_2 adsorption is affected by the temperature and CO_2 concentration, the CO_2 adsorption capacities of synthesized samples at different temperatures and CO_2 partial pressures were measured. Fig. 4 shows the adsorption capacities of synthesized MgO at the temperatures of 50 °C and 100 °C respectively. First of all, among these three prepared MgO samples, MgO-MO had the largest CO_2 adsorption capacity of 7.59 wt% at 50 °C. The adsorption capacity of MgO-BMC (7.34 wt%) was a little smaller than MgO-MO and MgO-RF had the smallest adsorption capacity of 6.44wt%. Clearly, the adsorption capacities of different samples were correlated with their BET surface area. This is also observed in previous study[15, 16]. Larger specific surface area provides more active sites resulting in high CO_2 adsorption capacity. In particular, all these prepared samples yielded much higher capacity than did commercially available MgO because of large surface area. However, when the adsorption temperature increased to 100 °C, all prepared MgO samples showed a reduction in CO_2 adsorption capacity at 100 °C. The maximal decrease of the CO_2 adsorption capacity could reach 2.42 wt% for MgO-RF. This is because high temperature may provide more energy for CO_2 to be desorbed, lowering the adsorption capacity. It should be noted that at high temperature, MgO-BMC had the largest adsorption capacity of 5.99 wt%, which was slightly higher than MgO-MO of 5.64 wt%. There was no direct relation between the surface area and the CO_2 adsorption capacity at high temperature because the adsorption capacity was also affected by the surface chemistry under different precursor and synthesis process.[15] A comparison of CO_2 adsorption capacities of different MgO adsorbents reported and samples synthesized in this work is given in Table 2.It can be seen that the reported CO_2 adsorption capacities of most MgO materials synthesized without template method were not high but the MgO materials synthesized by template method had a highest CO_2 capacity of 11.5 wt%. However, these methods were usually time consuming and contained multiple procedures. An expensive template or toxic solvent

was often needed. These drawbacks hindered the wide application of MgO in CO_2 adsorption. In the present work, porous MgO with high surface area was synthesized which all possessed relatively high CO_2 adsorption capacities. More importantly, the synthesis process was simple and economic, which enhanced the possibility of porous MgO in CO_2 adsorption.

The selectivity of synthesized samples to CO_2adsorption is another important parameter to characterize the CO_2 adsorption performance, which was also investigated in this work. Fig. 5 shows the adsorption capacities of synthesized MgO at different concentration of feeding gas. When the CO_2 partial pressure was switched from 1 bar to 0.15 bar, the CO_2 adsorption capacities of three samples all decreased. The CO_2 adsorption capacities of MgO-MO and MgO-BMC were decreased to 7.35 wt% and 6.75 wt%, respectively. The decreasing amplitude of adsorption capacity between the two different CO_2 partial pressure was less than 10% indicating that the good selectivity of the prepared MgO towards CO_2. But MgO-RF had an almost one-third of decline in its adsorption capacity, meaning that its selectivity is weak. In conclusion, MgO-MO and MgO-BMC were suited to be used for capturing CO_2 from flue gas because of their good capacity and selectivity.

When using adsorbents for the CO_2 capture, except for the adsorption capacity, the adsorption mechanism also needs to be accounted, because the recycling use of adsorbents in real applications requires the desorption, which highly depends on the adsorption mechanism. It has been reported that there existed two desorption steps in the CO_2 desorption process corresponding to physisorption and chemisorption [16].In this study, the above results on the selectivity have given an evidence on the strong bond between synthesized MgO and CO_2 molecule, indicating that the CO_2 adsorption mainly relies on chemisorption. To further confirm this point, CO_2 desorption of synthesized samples was investigated by thermo-gravimetric curves. To do this, the sample was firstly heated to 400 °C to release the water and impurity adsorbed. Then the temperature decreased to 50 °C and the adsorption began. When the adsorption process finished, the feed gas switched from pure CO_2 to pure nitrogen. The results are presented in Fig. 6.It is obvious that all three samples had small weight decline.

After purging nitrogen for half an hour, the temperature started to increase from 50 °C to 450 °C with a temperature rising rate of 3 °C/min. The weight continued to decrease. From the weight variation, it can be concluded that the first weight decline and the second weight decline were correlated to the weak and strong bonds between MgO and CO_2 molecule, respectively, demonstrating that there were indeed two desorption steps in the CO_2 desorption process.

In this study, in situ FTIR spectrums were recorded for all samples to further distinguish the mechanism. Fig. 7 shows the in situ horizontal attenuated total reflectance Fourier transform infrared spectroscopy of the synthesized samples. The intensity of the transmittance peak is correlated with the amount of adsorbent, background atmosphere and the extinction coefficient of bond. The synthesized samples were measured in the same atmosphere with different sample weights. Hence, the intensities of transmittance peaks at same wavenumber may be different for different samples. But the adsorption mechanism and the scale of different mechanisms for one sample could be deduced according to the spectrum. It is known that all carbonate species are characterized by more than one IR band. Hence, a summary of different IR bands for different carbonate species was shown in Table 3. From the FTIR patterns it could be seen that transmittance peaks appeared at 840 cm^{-1}, 1650 cm^{-1} and 1417-1448 cm^{-1}, which could be assigned to bicarbonate. The transmittance peaks appeared at 860 cm^{-1}, 1300-1370 cm^{-1} and 1520-1550 cm^{-1} indicated the existence of monodentate carbonate. Besides, combined with peaks at 830-850 cm^{-1}, 1310-1345 cm^{-1} and 1625-1670 cm^{-1}, bidentate carbonate could be verified on the synthesized samples. However, small band was also observed at 2303 cm^{-1}, which indicated the existence of physisorption of carbon dioxide. Combining the desorption curve with FTIR spectroscopy results, it is revealed that the adsorption mechanism of synthesized samples is mainly chemisorption but with small fraction of physisorption. Afterwards, CO_2 temperature programmed desorption was also used to evaluate the species and amount of different adsorption sites in this work. As shown in Fig. 8, the desorption curves of all MgO samples exhibited three peaks corresponding to three different types of binding sites. Besides, the predominant

desorption peak of MgO-RF appeared at low and medium temperature, while MgO-MO at medium temperature and MgO-BMC at high temperature, which demonstrated that MgO-RF could regenerate at low desorption temperature. Furthermore, the adsorption sites of all synthesized MgO samples can be desorbed below 280 °C which indicated that the synthesized samples could be regenerated at relatively low temperature. This is favorable for the industrial application of MgO adsorbent.

In addition to the adsorption capacity, selectivity and cycle stability, the adsorption kinetics is also investigated in this work. Since the MgO-MO showed the best performance in present study, only its adsorption kinetics was measured and compared with the commercially available MgO. Fig. 9 shows the adsorption curves of MgO-MO and commercially available MgO at 50 °C. The CO_2 capacity of MgO-MO finally reached to 7.59 wt% in about 4 hours which was 3 times higher than that of the commercially available MgO(2.2 wt%). Hence, it is revealed that MgO prepared by the synthesis method can largely improve the CO_2 adsorption capacity. From Fig. 9 it can also be seen that commercially available MgO achieved adsorption equilibration in less than one hour. But for MgO-MO,4 hours were not enough to achieve adsorption equilibration, meaning that synthesized MgO microparticles needed more time to achieve adsorption equilibration. Package of MgO microparticles tended to form highly porous structure with narrow pores. The mass transfer resistance of CO_2 was increased in such a structure, hindering CO_2 molecules to contact with the active sites. Thereby, more time is needed for MgO-MO to achieve adsorption equilibration. Because an effective adsorbent should have enough adsorption capacity with optimal accessibility to realize fast adsorption, open framework structure or appropriate pore size distribution is desired in the future.

4. Conclusion

In this work, MgO with high specific surface area was synthesized by the simple and economic methods without template. No expensive or toxic reagent was used. Experimental results reveal that the synthesized sample had relatively high CO_2 adsorption capacity as a result of high specific area and good selectivity to CO_2. FTIR

experiment demonstrated that the main adsorption mechanism of MgO was chemisorption. But there was still a friction of physisorption existed. CO_2-TPD curves of synthesized MgO samples revealed that CO_2 molecule was adsorbed on the surface of MgO in three different types of binding sites and the synthesized MgO could be regenerated at relatively low temperature. It should be noted that the prepared MgO needed more time to achieve adsorption equilibration. Hence, to achieve high adsorption capacity and rapid adsorption equilibration, a porous MgO structure with open framework structure or appropriate pore size distribution is needed.

Acknowledgements

This work is supported by Natural Science Foundation of China(No. 51276205), the State Key Program of National Natural Science of China (No. 51136007), the Research Project of Chinese Ministry of Education (No. 113053A), National Natural Science Funds for Distinguished Young Scholar (No. 51325602) and the key program of Natural Science Foundation of Chongqing (No. cstc2013jjB9004).

References

1. C. Stewart and M.-A. Hessami, *Energy Conversion and Management*, 2005, 46, 403-420.
2. M. Hasib-ur-Rahman, M. Siaj and F. Larachi, *Chemical Engineering and Processing: Process Intensification*, 2010, 49, 313-322.
3. Z. L. Zhao, X. Y. Cui, J. H. Ma and R. F. Li, *Int. J. Greenh. Gas Control*, 2007, 1, 355-359.
4. S. Choi, J. H. Drese and C. W. Jones, *ChemSusChem*, 2009, 2, 796-854.
5. D. P. Harrison, 2004.
6. Z. Yong, V. G. Mata and A. E. Rodrigues, *Adsorpt.-J. Int. Adsorpt. Soc.*, 2001, 7, 41-50.
7. D. Bonenfant, M. Kharoune, P. Niquette, M. Mimeault and R. Hausler, *Sci. Technol. Adv. Mater.*, 2008, 9.
8. Z. Yong and A. E. Rodrigues, *Energy Conversion and Management*, 2002, 43, 1865-1876.
9. S. P. Wang, S. L. Yan, X. B. Ma and J. L. Gong, *Energy Environ. Sci.*, 2011, 4, 3805-3819.
10. J. Liu, P. K. Thallapally, B. P. McGrail and D. R. Brown, *Chem. Soc. Rev.*, 2012, 41, 2308-2322.
11. B. Feng, H. An and E. Tan, *Energy Fuels*, 2007, 21, 426-434.
12. Q. A. Wang, J. Z. Luo, Z. Y. Zhong and A. Borgna, *Energy Environ. Sci.*, 2011, 4, 42-55.
13. Y. Duan and D. C. Sorescu, *The Journal of chemical physics*, 2010, 133, 074508.
14. M. Bhagiyalakshmi, J. Y. Lee and H. T. Jang, *Int. J. Greenh. Gas Control*, 2010, 4, 51-56.
15. Z. Zhao, H. Dai, Y. Du, J. Deng, L. Zhang and F. Shi, *Materials Chemistry and Physics*, 2011, 128, 348-356.
16. A. M. Ruminski, K.-J. Jeon and J. J. Urban, *J. Mater. Chem.*, 2011, 21, 11486-11491.
17. F. Meshkani and M. Rezaei, *Powder Technol.*, 2010, 199, 144-148.
18. S. W. Bian, J. Baltrusaitis, P. Galhotra and V. H. Grassian, *J. Mater. Chem.*, 2010, 20, 8705-8710.
19. P. Ouraipryvan, T. Sreethawong and S. Chavadej, *Materials Letters*, 2009, 63, 1862-1865.
20. K. K. Han, Y. Zhou, W. G. Lin and J. H. Zhu, *Microporous and Mesoporous Materials*, 2012.
21. J. K. Bartley, C. Xu, R. Lloyd, D. I. Enache, D. W. Knight and G. J. Hutchings, *Applied Catalysis B: Environmental*, 2012, 128, 31-38.
22. S. Ward, J. Braslaw and R. Gealer, *Thermochimica Acta*, 1983, 64, 107-114.
23. S. C. Lee, H. J. Chae, S. J. Lee, B. Y. Choi, C. K. Yi, J. B. Lee, C. K. Ryu and J. C. Kim, *Environmental science & technology*, 2008, 42, 2736-2741.
24. L. Li, X. Wen, X. Fu, F. Wang, N. Zhao, F. Xiao, W. Wei and Y. Sun, *Energy Fuels*, 2010, 24, 5773-5780.
25. H. Jeon, Y. J. Min, S. H. Ahn, S.-M. Hong, J.-S. Shin, J. H. Kim and K. B. Lee, *Colloids and Surfaces A: Physicochemical and Engineering Aspects*, 2012.
26. Y. Y. Li, M. M. Wan, W. G. Lin, Y. Wang and J. H. Zhu, *Journal of Materials Chemistry A*, 2014, 2, 12014-12022.
27. J. A. C. Lercher, C.; Noller, H., *J. Chem. Soc.*, 1984, 80.
28. J. Evans and T. Whateley, *Trans. Faraday Soc.*, 1967, 63, 2769-2777.
29. G. Busca and V. Lorenzelli, *Materials Chemistry*, 1982, 7, 89-126.

Figure captions

Fig. 1 XRD patterns of MgO-MO, MgO-BMC and MgO-RF.

Fig. 2 SEM images of (a) MgO-MO; (b) MgO-BMC; (c) MgO-RF; (d) MgO-CA.

Fig. 3 Nitrogen adsorption-desorption isotherms and pore size distributions (inset) of MgO-MO, MgO-BMC, MgO-RF and MgO-CA.

Fig. 4 CO_2 adsorption capacities of MgO at different adsorption temperatures.

Fig. 5 CO_2 adsorption capacities of MgO at different concentrations of feed gas.

Fig. 6 Thermo gravimetric curves during adsorption-desorption process.

Fig. 7 In situ horizontal attenuated total reflectance (HATR) Fourier transform infrared spectroscopy of samples.

Fig. 8 CO_2 –TPD profiles of the MgO samples.

Fig. 9 Adsorption curves of MgO-MO and commercially available MgO at 50 °C, CO_2 partial pressure of 1bar, respectively.

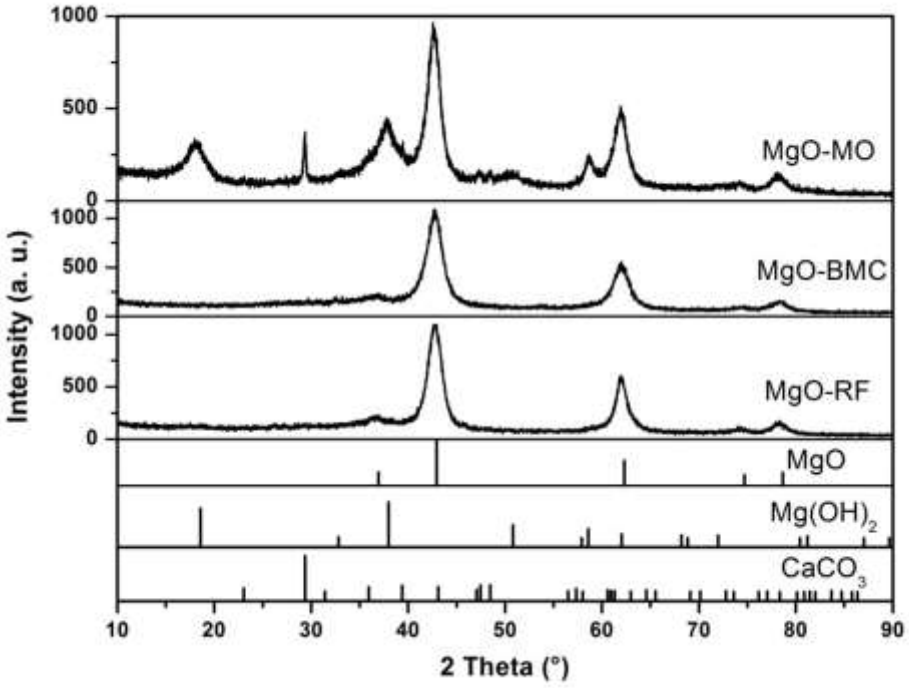

Fig. 1 XRD patterns of MgO-MO, MgO-BMC and MgO-RF.

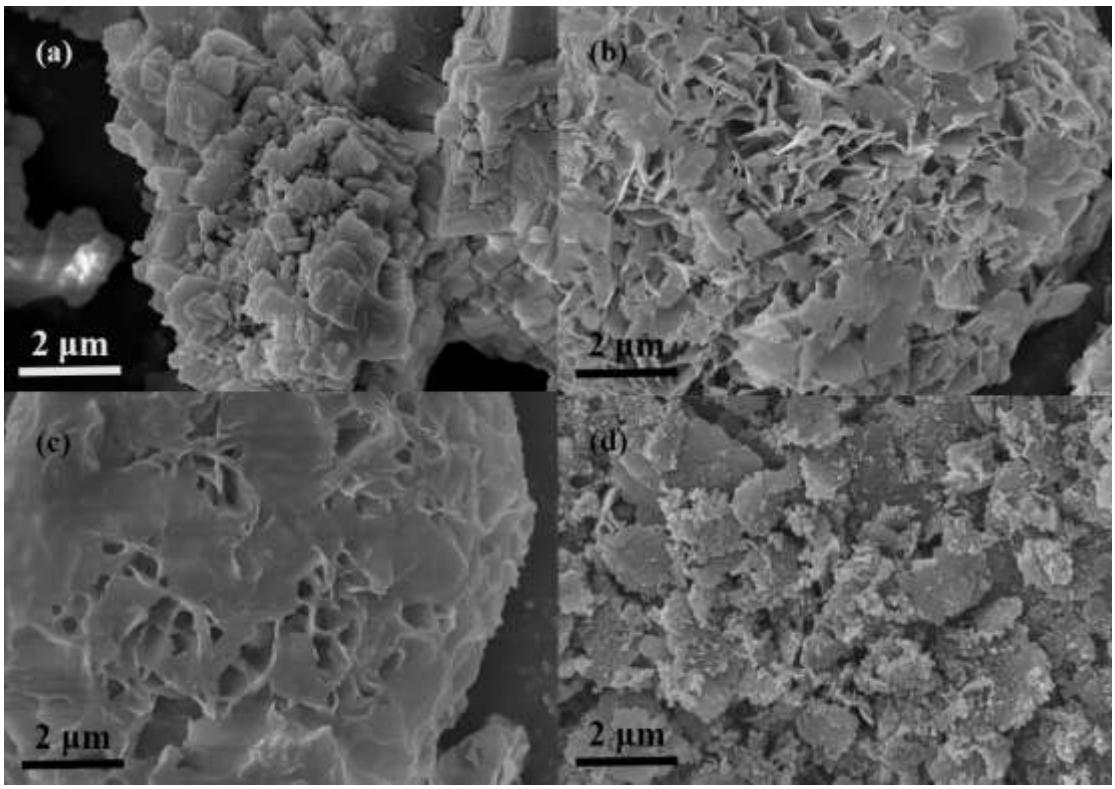

Fig. 2 SEM images of (a) MgO-MO; (b) MgO-BMC; (c) MgO-RF; (d) MgO-CA.

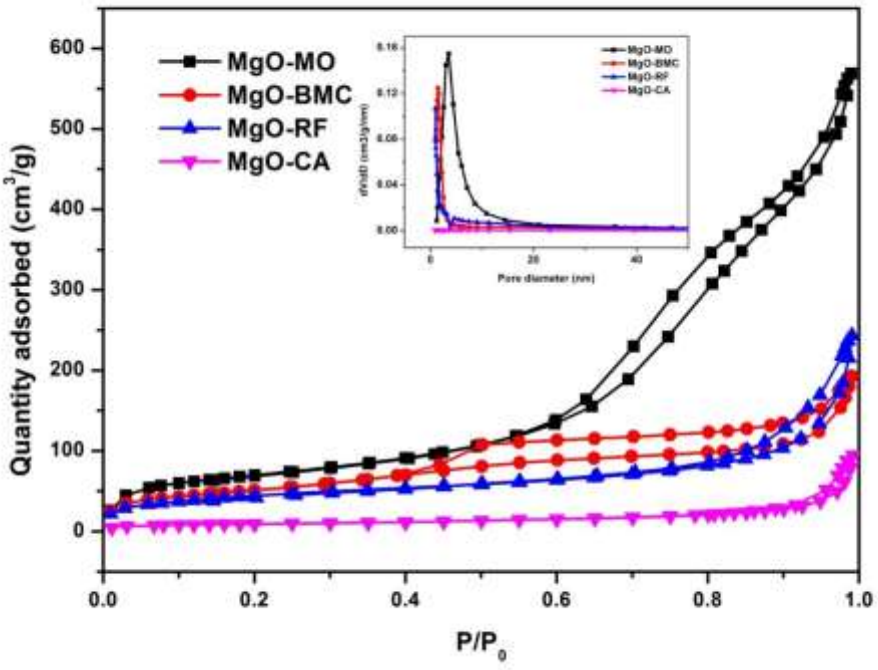

Fig. 3Nitrogen adsorption-desorption isotherms and pore size distributions (inset) of MgO-MO, MgO-BMC, MgO-RF and MgO-CA.

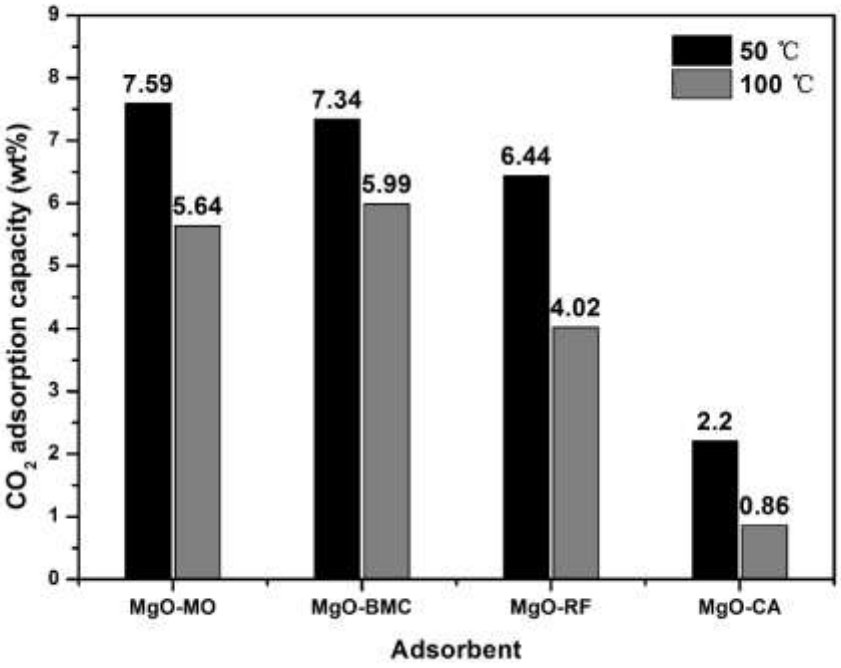

Fig. 4 CO_2 adsorption capacities of MgO at different adsorption temperatures.

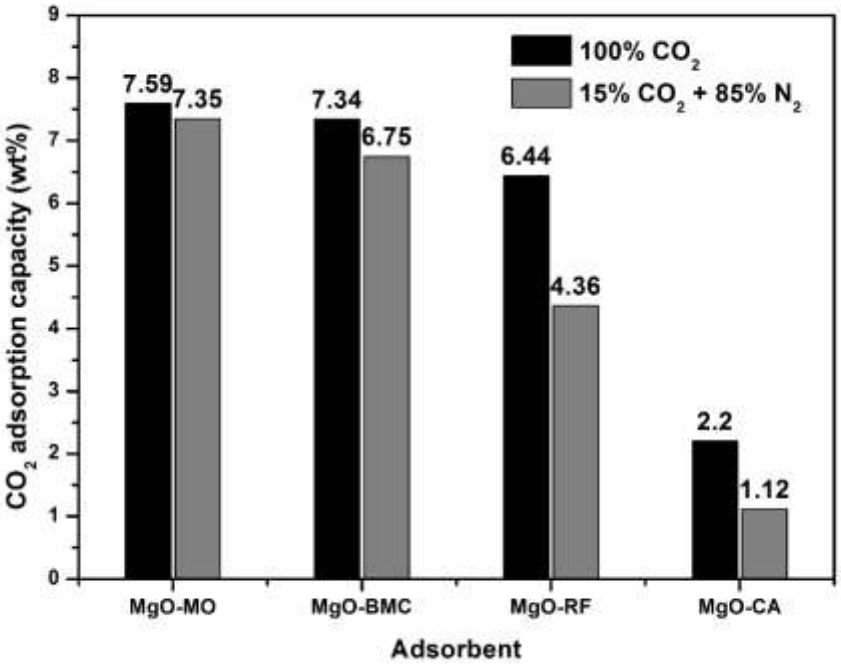

Fig. 5 CO_2 adsorption capacities of MgO at different concentrations of feed gas.

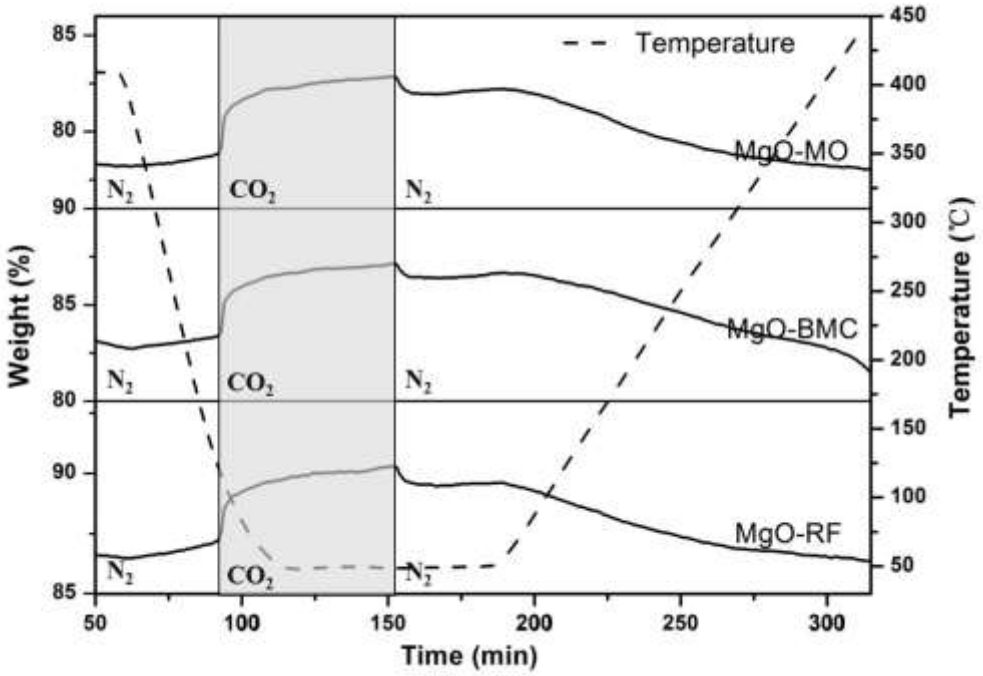

Fig. 6 Thermo gravimetric curves during adsorption-desorption process.

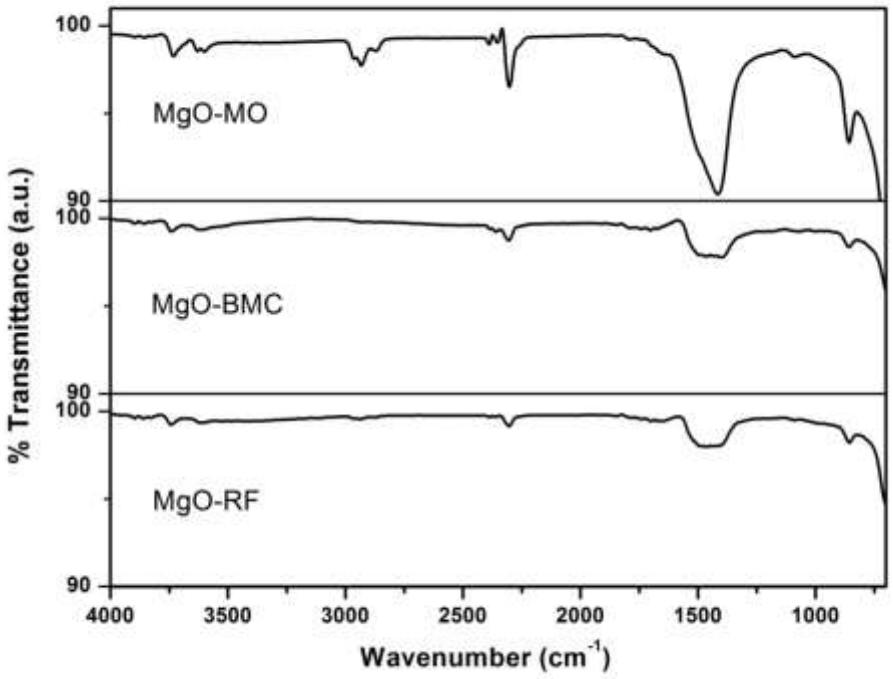

Fig. 7 In situ horizontal attenuated total reflectance (HATR) Fourier transform infrared spectroscopy of samples at room temperature and a CO_2 flowrate of 20 mL/min.

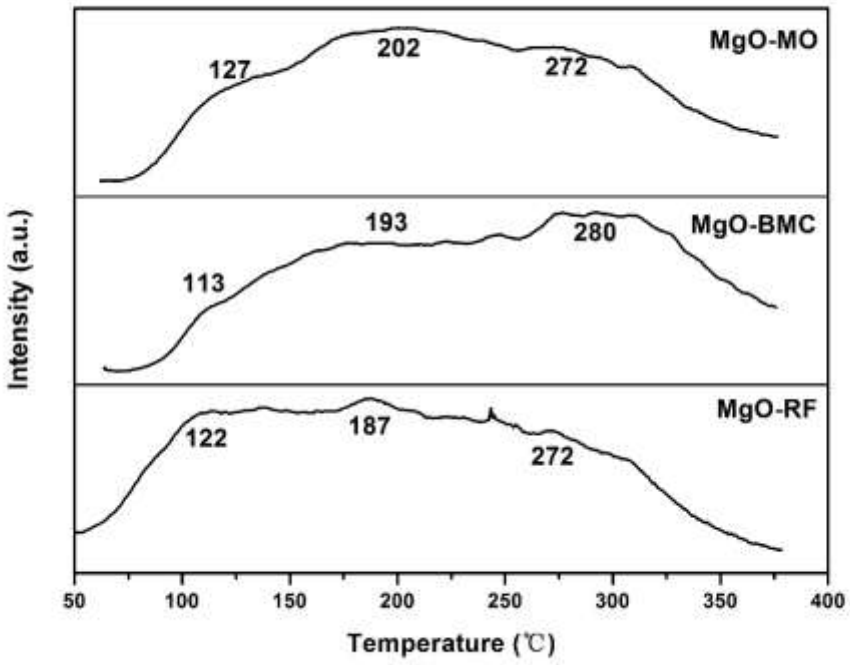

Fig. 8 CO_2 –TPD profiles of the MgO samples.

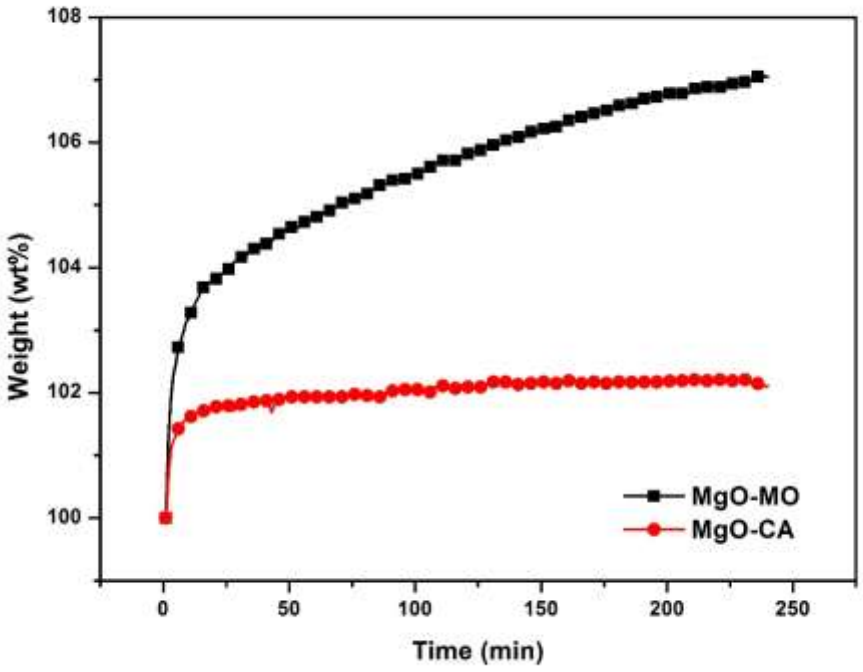

Fig. 9 Adsorption curves of MgO-MO and commercially available MgO at 50 °C, CO_2 partial pressure of 1bar, respectively.

Table 1
Porous structure parameters determined from nitrogen adsorption-desorption isotherm.

Sample	BET surface area m^2/g	Pore volume cm^3/g	Pore size nm
MgO-BMC	210	0.250	4.7
MgO-RF	161	0.266	6.6
MgO-MO	252	0.763	12.1
Commercial MgO	32	0.076	9.3

Table 2
A summary of CO_2 adsorption capacities on different MgO sorbents.

material	synthesis method	surface area m^2/g	adsorption condition	adsorption capacity wt%	reference
MgO	(-)	210	60°C, 2h	0.7	16
MgO	hydrothermal	203	RT, 1h	1.62	15
MgO	decomposition	(-)	0°C, 0.2 bar, 24h	2.8	22
MgO	(-)	(-)	60 °C, 160 min	6.4	23
MgO/Al_2O_3	impregnation	200	60°C,1 bar, 1h	5.98	24
MgO/TiO_2	sol-gel	101	25°C,1 bar, 550 min	2.01	25
porous MgO	template	250	25°C,1 bar, 1h	8	14
porous MgO	template	250	100°C,1 bar, 1h	10	14
porous MgO	template	130	100°C,1 bar, 1h	11.5	20
porous MgO	decomposition	336	200°C,1 bar	2.89	26
porous MgO	decomposition	252	50°C,1 bar	7.59	present work

(-):No mentioned

Table 3
IR band positions (cm^{-1}) of different carbonates on MgO

Bibarbonate	Monodentate carbonate	Bidentate carbonate	Reference
1650 1417-1448 1220-1229	1538-1580 1420	1700 1357-1380	27
1655 1405 1220 1040 840	1510 1390 1035 865	1665 1325 1005 850	28
	1050	1005-950	29

860	850-830
1520-1550	1625-1670
1390-1410	1275-1325

Highly porous MgO were synthesized for CO_2 adsorption by simple and economic thermal decomposition of different precursors. The synthesized MgO exhibited highly porous structure and high BET surface area in a range of 161-252 m^2g^{-1}. Besides, the synthesized MgO not only showed good selectivity to CO_2 but also yielded a CO_2 adsorption capacity of as high as 7.59 wt%, which was attributed to chemisorption according to in situ FTIR and CO_2 TPD curves. This work provides a new way to synthesized MgO with highly porous structure for CO_2 adsorption.